Laser Sideband Spectrometer: A new spectrometer concept with very large bandwidth

R. Schieder, O. Siebertz, F. Schloeder, P. Nagy

KOSMA, I. Physikalisches Institut, Universität zu Köln, Germany

Abstract

A new concept of a super wideband spectrometer is presented, which is based on phase-modulation of a single mode laser. The sideband spectrum is analyzed by means of a simple plane-parallel Fabry-Perot interferometer. A first prototype spectrometer has been built with a bandwidth of about 12 GHz and a resolution of 100 MHz. It has been demonstrated that the concept is viable and ready for further usage in very large IF-bandwidth heterodyne systems.

Introduction

The trend to higher frequencies in heterodyne remote sensing causes high demand for larg bandwidth of the back-ends of such systems. Nowadays the typical bandwidth of a suitable back-end is of the order of 1 GHz, but the latest generation of heterodyne receivers has an IF bandwidth of 4 GHz or even more, like is used in the HIFI instrument of ESAs Herschel mission. On the other hand, the linewidth of pressure broadened atmospheric lines may reach values near 10 GHz so that back-ends with very large bandwidth are needed, while high resolution is not always required. The same is true for extragalactic signals when observing at frequencies of several THz. It is very difficult to achieve such large instantaneous spectrometer bandwidth with any present technology. There are a couple of different methods for large bandwidth, such as the analogue correlator (WASP), dedicated filterbanks, hybrid spectrometers based on correlator or acousto-optical methods (e.g. WBS in HIFI, see Poster P-14 on this conference), or recently, the introduction of a new Bragg-cell material for a broad band AOS [See paper 8-4 on this conference]. Nevertheless, none of these technologies have succeeded so far to provide access to very large instantaneous bandwidth in or above the 10 GHz range.

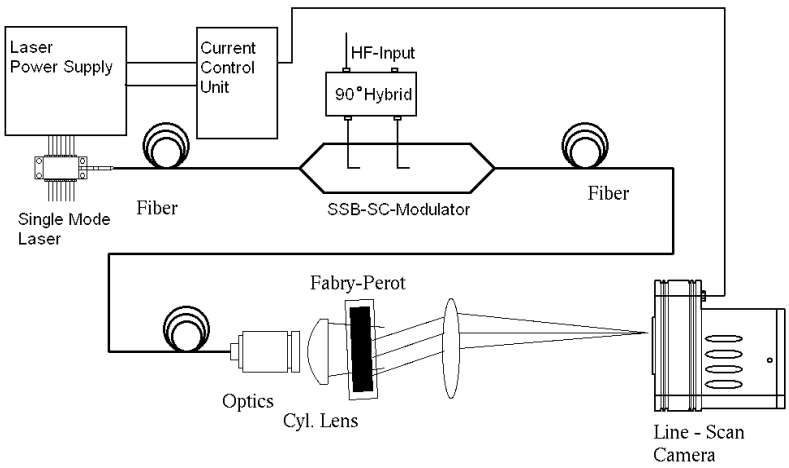

Fig.1

Scheme of the Laser Sideband Spectrometer. It consists of a single mode laser, an electro-optical phase-modulator and a custom made Fabry-Perot interferometer.

We have pursued a new idea for such instrument which is based on simple optical methods. The narrow line of a single mode laser is modulated by means of an electro-optical phase modulator. The generated sidebands contain all spectral information of the electric signal, which is driving the modulator. Consequently, it is natural to analyse the spectral distribution of the sidebands by means of a Fabry-Perot interferometer (FPI). Modulators are available with a bandwidth of more than 20 GHz, while the FPI is available as custom made item with nearly any bandwidth depending on the spacing of the mirrors in the device. With new coatings very high finesse in the range of a few hundred can be achieved so that spec-

trometers with reasonable numbers of resolution elements are accessible at practically any desired total bandwidth.

The principle of the Laser Sideband Spectrometer (LSS) is depicted in Fig.1. We use a near-IR laser at 1.55 µm wavelength and about 80 mWatts output power. The modulator is a single sideband modulator, which suppresses the initial laser carrier at the same time. Thus, real SSB operation is available. This is important, because with a DSP modulator, only half of the free spectral range (FSR) of the FPI would be available for the spectral analysis due to overlapping upper and lower sideband signals from successive orders of the FPI. The output of the modulator is then coupled to the FPI by special optics in order to obtain maximum efficiency (see below). The final imaging optics concentrates the signal light onto a linear diode array, which is controlled and processed by similar electronics as we use for our acousto-optical spectrometers as well.

Concept analysis

The plane-parallel Fabry-Perot interferometer needs some particular attention. As is immediately deducible from diffraction arguments and from walk-off problems within the interferometer, there is a minimum diameter D needed for a given free spectral range FSR and finesse F like

$$D \geq \sqrt{2 \cdot \lambda_{Laser} / FSR} \cdot F$$

For example, for a wavelength of λ_{Laser} = 1.55 µm, a FSR of 0.5 cm^{-1} (15 GHz) and a finesse of 200, the needed diameter is 5 cm! This means that very high accuracy for the fabrication of such FPI is required. A too small diameter causes sidelobe ringing of the signal and reduction of resolution. On the other hand, for such relatively high finesse, it is essential that extremely loss-free coatings are used. Otherwise, the throughput of the FPI, and therefore the efficiency of the optics become seriously reduced.

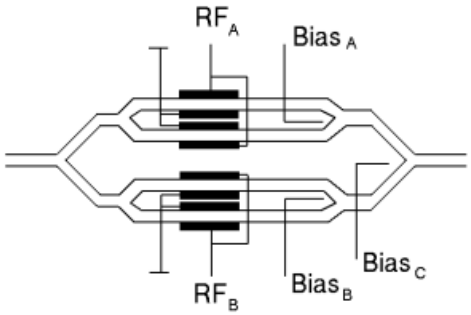

Fig.2

Scheme of the single sideband modulator. In the two sub-interferometers the laser carrier is suppressed to better than -20 dB. The two RF-inputs need to be phase shifted by π/2 by means of an RF hybrid. In the combining interferometer the two outputs are co-added with a phase delay of π/2. This can be controlled by a third dc-bias. For further details see text.

The principle of the modulator is shown in Fig.2. It consists of three different two beam interferometers, which can be tuned by means of separate dc voltages. In the two sub-interferometers the AC signal introduces a phase modulation of the laser light in both interferometer arms. The optical pathlength difference of these interferometers is set to $\lambda_{Laser}/2$ minimizing the laser carrier output to nearly zero level. This is important, because the wings of the FPI response to the strong laser carrier could add a severe background to the sideband signal resulting in additional and unwanted shot noise in the output of the spectrometer (see below). In order to explain the single sideband behaviour we need to use a bit of mathematics. The phase modulation with an IF frequency ω of the laser amplitude at frequency Ω in both arms of the first sub-interferometer can be described by:

$$A_1(t) = A_0 \cdot \exp\{i \cdot [\Omega \cdot t \pm u \cdot \cos(\omega \cdot t)]\} = A_0 \cdot \sum_{n=-\infty}^{\infty} (\pm i)^n \cdot J_n(u) \cdot \exp\{i \cdot [\Omega + n \cdot \omega] \cdot t\}$$

u is the modulation amplitude and the $J_n(u)$ are the integer Bessel-functions of order n. Due to the opposite sign of the modulation in both arms only odd contributions in the sum remain, when recombined at a pathlength difference of λ/2. In particular, the zero order carrier $J_0(u)$ is removed by this setting. The signal input to the second interferometer is phase shifted by 90 degrees. Therefore we have here:

$$A_1(t) = A_0 \cdot \exp\{i \cdot [\Omega \cdot t \pm u \cdot \sin(\omega \cdot t)]\} = A_0 \cdot \sum_{n=-\infty}^{\infty} (\pm 1)^n \cdot J_n(u) \cdot \exp\{i \cdot [\Omega + n \cdot \omega] \cdot t\}$$

Again, all even orders disappear after recombination in the sub-interferometer. The two interferometer output amplitudes are then co-added in the combining interferometer at 90 degrees phase shift (optical pathlength difference = λ/4), which multiplies the second amplitude by $exp[i \cdot \pi/2] = i$, so that all orders in the sum of both interferometer outputs disappear except for $n = 4k+1$ with $k = 0, \pm1, \pm2, \ldots$ The lowest order remaining is that for $n = 1$ ($k = 0$), which is the upper sideband. For a pathlength difference of -λ/4, the lower sideband is left. The sideband suppression is specified to better than 20 dB.

The higher order terms $J_{4k+1}(u)$, $k = \pm1, \pm2, \ldots$ are causing harmonic response of the modulator, and it is therefore essential to keep them small. The lowest term is $J_{-3}(u)$ which is for low modulation amplitude reduced in comparison to $J_1(u)$ by a factor of u^2, so that it is not difficult to avoid such contributions. At the same time, non-linearity due to compression should stay below 1% for a decent spectrometer, i.e. the value of u should stay below 0.2, which corresponds to maximum phase amplitude of less than 3% of a wavelength. On the other hand, since for a broad band spectrum all frequency components contribute identically to the compression, it is possible to correct afterwards for linear response by software, when calibrating the deviation from linearity beforehand. Therefore it is still possible to operate at much higher modulation index than stated before. This helps to improve the efficiency of the system.

When analysing RF-signals by optical means, it is important to note that the shot noise might become the dominant problem. For example, if we consider a LSS with 15 GHz bandwidth and a finesse of 200, we have resolution element bandwidth of $\Delta_{1/2}$ = 15GHz/200 = 75 MHz. The radiometric noise level is determined by the fluctuation bandwidth (rms ~ $\sqrt{B_{FI}}$), which is in this case roughly 200 MHz ($B_{FI} = \pi \cdot \Delta_{1/2}$). On the other hand, the shot noise level is determined by the number N of photo-electrons per second (rms ~ $\sqrt{N}$). The shot noise should stay smaller than the radiometric noise for a suitable spectrometer so that we need at least $4 \cdot 10^8$ photo-electrons per second and pixel when assuming a noise dynamic range of the instrument of 10 dB for example. If we use 500 diodes of a diode array, the total optical power at the detectors must be larger than 0.4 μWatt. For a laser with 80 mWatt it requires an optical efficiency of about 10^{-5}. This is well within the limits of linear operation of the modulator.

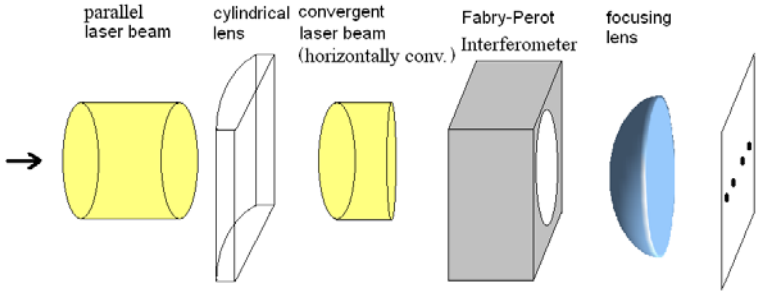

Fig.3

Layout of the LSS optics. The spectral distribution of the signal light is concentrated on a line matching the linear CCD.

It is also useful to design the coupling optics appropriately. In order to observe resonances for all sideband frequencies within the bandwidth of the spectrometer, the divergence of the incoming laser beam needs to be well defined. One finds that for a FPI with above defined parameters a minimum divergence of the laser beam of 0.7 degrees, when observing the spectrum in lowest FPI order. On the other hand, it is not desirable to waste signal light while generating rings of light as is normal for a FPI. Therefore we use an astigmatic light distribution as input to the FPI, which is achieved by inserting an additional cylindrical lens with large focal length. The situation is depicted in Fig.3. The horizontal beam divergence is adjusted for minimum divergence, so that in effect a linear cut through the image circles of the FPI is finally illuminated in the image plane at the CCD.

The frequency calibration of a FPI output is strongly non-linear. The frequency is a quadratic function of the distance from the optical axis of the FPI, i.e. the pixel number of the diode array. Therefore, resampling of the frequencies is essential. In order to avoid unfavourable losses in resolution, the optical resolution on the diode array is chosen for oversampling the spectrum accordingly. In combination with a suitable resampling procedure using a Gaussian weighting function one obtains a very linear frequency scale together with sufficient frequency resolution. The effect of the resampling is demonstrated in Fig.4.

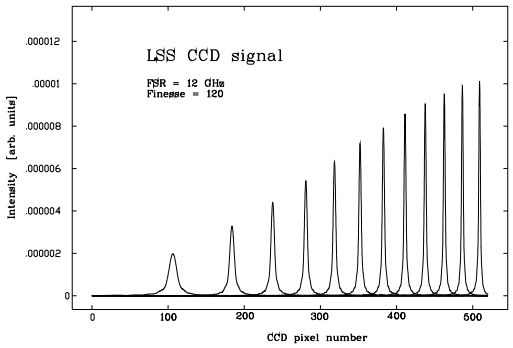

Fig.4a
Comb spectrum seen with the LSS before resampling. The non-linear frequency scale is very obvious.

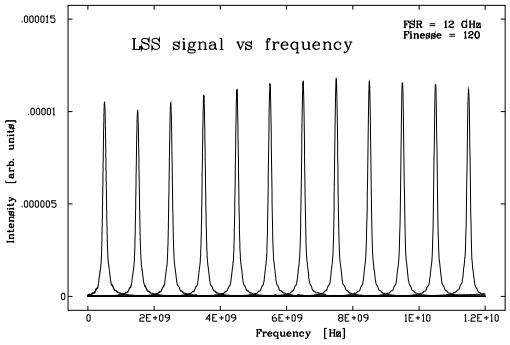

Fig.4b
Comb spectrum seen with the LSS after resampling. Note the modified power distribution.

First Results

The prototype LSS is shown in Fig.5. The laser is located at the right on the base plate. The light is coupled to the modulator at the outer side of the back wall of the unit through a fiber, and its output is then brought into the unit back again by fiber. The emission from the fiber is then astigmatically formed as input to the FPI by the illuminating optics. Behind the FPI a simple imaging telescope is used illuminating the diode array.

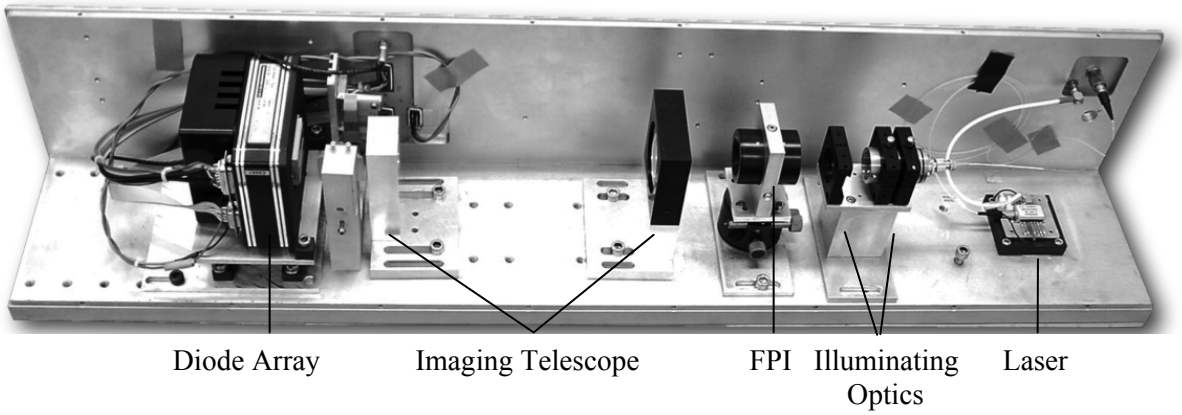

Fig.5 Optics unit of the prototype LSS

It is important that the carrier suppression in the two sub-interferometers is efficient. To demonstrate this, Fig.6 shows spectra taken with and without proper biasing of the interferometers. The resolution function of FPIs, the Airy-functions, decrease with distance Δx from center like $1/\Delta x^2$ so that extended wings of the laser carrier could lead to a strong background signal, which contributes to the shot noise of the detectors. This one must avoid, therefore, proper tuning of the interferometer bias is important.

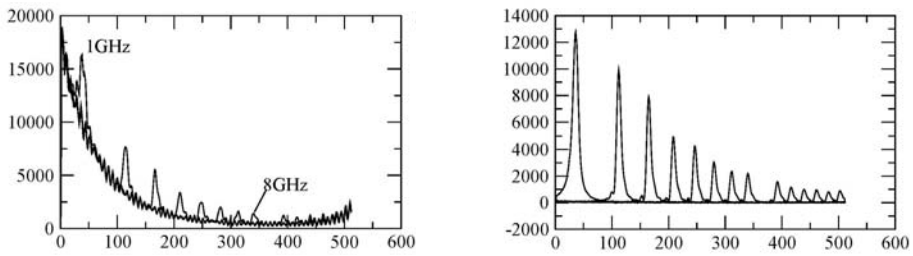

Fig.6: Demonstration of the carrier suppression in the two sub-interferometers. The lower frequencies (low pixel numbers) in the spectra are affected strongly by background, as is seen in the left plot..

The inevitable thermal drifts of laser and FPI resonance frequencies need a regulator in order to keep the spectral features at constant position on the diode array. For this, two pixels of the diode array are used, which detect the residual light of the carrier at two sides of its FPI resonance. By means of a differential amplifier, a regulator signal is derived which is fed to the laser current supply.

Fig.7 shows the output of an 18 GHz FPI with white noise input from a noise source after resampling. The bandpass is reasonably flat, and improvements are still possible by means of a RF-equalizer. This demonstrates that very large bandwidth is indeed obtainable.

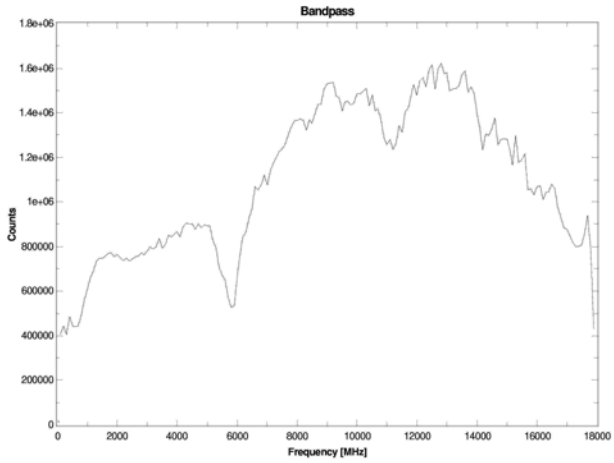

Fig.7

Bandpass of the LSS seen with an 18 GHz FPI and SSB modulator.

Finally, the stability of the spectrometer is most important. Since the LSS has large fluctuation bandwidth, the radiometric noise level is less than 10% of that of one of our standard AOSs. This means that the drift noise in the electronics as well as the amplitude stability of the laser must be more stable accordingly. This is a particular challenge for the instrument development. Fig.9 shows an Allan variance plot, as we have achieved so far. It is by now means perfect yet! The dependence on integration time like $1/\sqrt{t_{Int}}$ is somewhat surprising, and it seems to indicate that there is some noise contribution which follows approximately a $1/f^{1/2}$ spectral distribution, which we have not seen in other spectrometers. We believe that the laser is responsible for this behaviour, and we are presently improving the laser frequency and amplitude stability. We assume that in short time a fully qualified back-end is available, and we are hoping that a heterodyne receiver with 12 GHz IF bandwidth will become available for a realistic observing run.

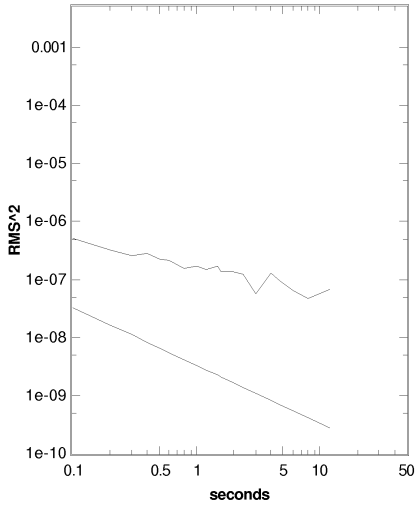

Fig.8

Allan variance plot of the LSS output. The slope indicates that there exists some unwanted instrumental noise of unknown origin. At longer integration times the drift noise starts to dominate. The figure indicates that the stability of the instrument still needs some improvement.